*Journal of Microscopy, Vol. 200, Pt 3, December 2000, pp. 179–186.*
*Received 23 May 2000; accepted 25 July 2000*

# Penetration pathways of fluorescent dyes in human hair fibres investigated by scanning near-field optical microscopy

A. KELCH*, S. WESSEL*, T. WILL*, U. HINTZE*, R. WEPF* & R. WIESENDANGER†
*Analytical Research, Beiersdorf AG, Department of Analytical Research, Troplowitzstr. 15, 22529 Hamburg, Germany
†Institute of Applied Physics, University of Hamburg, Germany

**Key words.** Confocal laser scanning microscopy (CLSM), fluorescent dye penetration, hairs, scanning near-field optical microscopy (SNOM).

## Summary

Thin cross-sections of human hairs were investigated by scanning near-field optical microscopy (SNOM) and confocal laser scanning microscopy (CLSM) after penetration of a fluorescent dye. The same samples were measured with both techniques to compare the observed structures. The images obtained from the two methods show nearly identical structures representing pathways of the dye molecules in hairs. The SNOM images provide a higher resolution than the CLSM images. Therefore, SNOM is believed to be a suitable method for investigations at a resolution of 100 nm on penetration pathways of fluorescent dyes such as the cell membrane complex pathway in cross-sections of hairs.

## Introduction

The cosmetics industry takes an interest in the penetration of several substances into hair fibres in order to improve its knowledge of diffusion processes in hairs. Penetration of ingredients of cosmetic products can influence the chemical and physical properties of hairs and thus change the consumer's impressions of, for example, colour and flexibility (Kaplin *et al.*, 1982; Robbins, 1988). To study the diffusion of molecules into hairs, fluorescent dyes are often used. In this case the penetration can be investigated by conventional light microscopy (LM) and confocal laser scanning microscopy (CLSM) (Corcuff *et al.*, 1993; Pötsch & Moeller, 1996).

Light microscopy is a well established tool for observing structures of biological samples. Structures of about 200 nm can theoretically be resolved with visible light using the Rayleigh criterion $\Delta r = 0.61\lambda/n\sin\alpha$ (Shotton, 1989) ($\Delta r$ = distance between two luminous points, $\lambda$ = wavelength of light, $n$ = refractive index of the medium between sample and objective, $\alpha$ = half of the aperture angle of the objective). In practice, only CLSM can achieve this resolution on thick samples. The improved resolution by a factor of about $\sqrt{2}$ in CLSM originates from the illumination of the sample and detection of the emitted light at the same focal plane in the sample (Shotton, 1989). However, both imaging modes are limited in resolution by the wavelength of light.

Scanning near-field optical microscopy (SNOM) was developed to overcome the wavelength dependence of the resolution (Pohl *et al.*, 1984; Dürig *et al.*, 1986). In near-field optics the sample is scanned in close proximity to a small light source. In general the light source is made of a tapered glass-fibre coated with aluminium, providing aperture sizes of 50–100 nm at the apex. During scanning the distance between probe tip and sample is kept constant by shear force mode (Karrai & Grober, 1995). For distances much smaller than $\lambda$ only light in the vicinity of the aperture interacts with the sample. Therefore the far-field phenomenon of diffraction does not occur and the resolution depends only on the aperture size and the probe–sample distance. Resolutions well below the diffraction limit (down to 12 nm) have been achieved by this technique (Betzig & Trautmann, 1992).

Human hairs consist of keratinized cells forming a fibre with two main regions (Fig. 1a). The cortex contains elongated cortical cells, which mostly have a tapered shape with fringes at their ends (Fig. 1c) (Kassenbeck, 1991). Their inner structure is fibrillar. The macrofibrils (0.4 μm diameter) consist of intermediate filaments (~10 nm diameter), which are embedded in sulphur-rich matrix proteins. Each cortical cell is surrounded by a chemically resistant membrane (cornified envelope), which belongs to the cell membrane complex (CMC). The CMC also contains intercellular proteins with low sulphur content, and lipids (Zahn, 1984; Wortmann *et al.*, 1997).

Correspondence to: Alexander Kelch. Tel: +49 40 49 096638; fax: +49 40 49093855; e-mail: kelcha@hamburg.beiersdorf.com

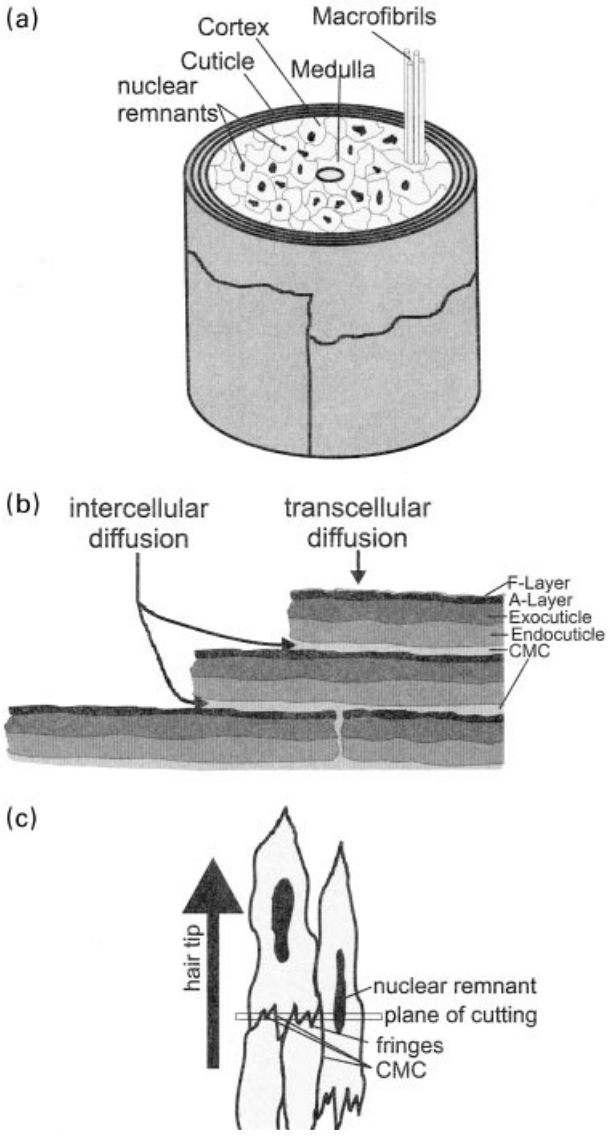


**Fig. 1.** (a) A model of human hair shows the main morphological structures of the inner region (Robbins, 1998). (b) Schematic drawing of the two major diffusion pathways of dye molecules into hair fibres (Robbins, 1998). (c) Model of a longitudinal section across cortical cells. The indicated cutting plane across the cortical cells provides a variety of structures in cross-section.

The cuticle is a surrounding layer of flattened overlapping cells. Each cell shows a layered structure consisting of three major parts. First, the highly crosslinked epicuticle consists of a thin lipid layer (F-layer) and a sulphur-rich protein layer (A-layer). Second, the adjacent exocuticle (containing half as much sulphur) is also highly crosslinked. The underlying third layer, the endocuticle, contains remnants of cell organelles and has a low sulphur content. The endocuticle and the CMC with its intercellular material are soft and characterized by a large potential for swelling in aqueous solutions (Robbins, 1988; Zahn *et al.*, 1997) (Fig. 1b).

Two major diffusion pathways into hair fibres exist. The transcellular route describes the pathway across low and high sulphur parts of the cuticle cells. This pathway is important especially for small hydrophilic molecules. An alternative way is intercellular diffusion, which is preferred for large hydrophobic or apolar molecules such as fluorescent dyes. Molecules penetrate the cuticle via low sulphur regions of the cuticle, the intercellular material and endocuticle. Low sulphur regions can function as preferred diffusion pathways because of their swelling behaviour in aqueous solutions (Robbins, 1988). Under non-aqueous conditions molecules also diffuse through intercellular pathways; this can be explained by the high mobility of the lipid and protein molecules of the CMC at room temperature (Wortmann *et al.*, 1997). After penetrating the cuticle the molecules diffuse on the intercellular route of the cortex to the centre of the hair. Only after a long period of penetration do the molecules migrate also into the cortical cells (Kamath *et al.*, 1995). In general, the diffusion is a combination of both routes (Robbins, 1988) (Fig. 1b).

A precise description of the diffusion pathway in human hair, where structures below 200 nm are relevant, is not possible in conventional LM because of the diffraction limit. To achieve higher resolutions we investigated cross-sections of hairs by SNOM after penetration of a fluorescent dye. To our knowledge a penetration study on hairs by SNOM has not yet been presented. The images obtained were compared with CLSM images of the same samples with regard to contrast and resolution.

## Materials and methods

### *Sample preparation*

A freshly plucked European brown hair was immersed for 24 h at room temperature in a 1% octadecanoylaminofluorescein (Molecular Probes, Eugene, OR) solution in methanol. The specified maximal excitation and emission wavelengths of octadecanoylaminofluorescein in methanol are $\lambda_{ex} = 497$ nm and $\lambda_{em} = 518$ nm. After removing the excess dye from the hair surface by cleaning the hair in methanol for 10 s, the hair was air dried for at least 24 h. Then it was embedded in Epon resin for 3 days at 60 °C. 200 nm and 50 nm thin cross-sections were cut with an ultramicrotome (Leica, Bensheim, Germany) using a diamond knife. After this, the cross-sections were placed on a 0.1 mm thick coverslip.

### *SNOM*

A slightly modified commercially available SNOM (Topometrix, Pfungstadt, Germany) was used for the measurements on the cross-sections. The set-up is shown in Fig. 2. Light from an $Ar^+$-ion laser is launched into a single mode glass-fibre coupled to a SNOM probe. The probes consist of a tapered glass-fibre, coated with aluminium, that is attached to a quartz tuning fork with approximately 90 kHz

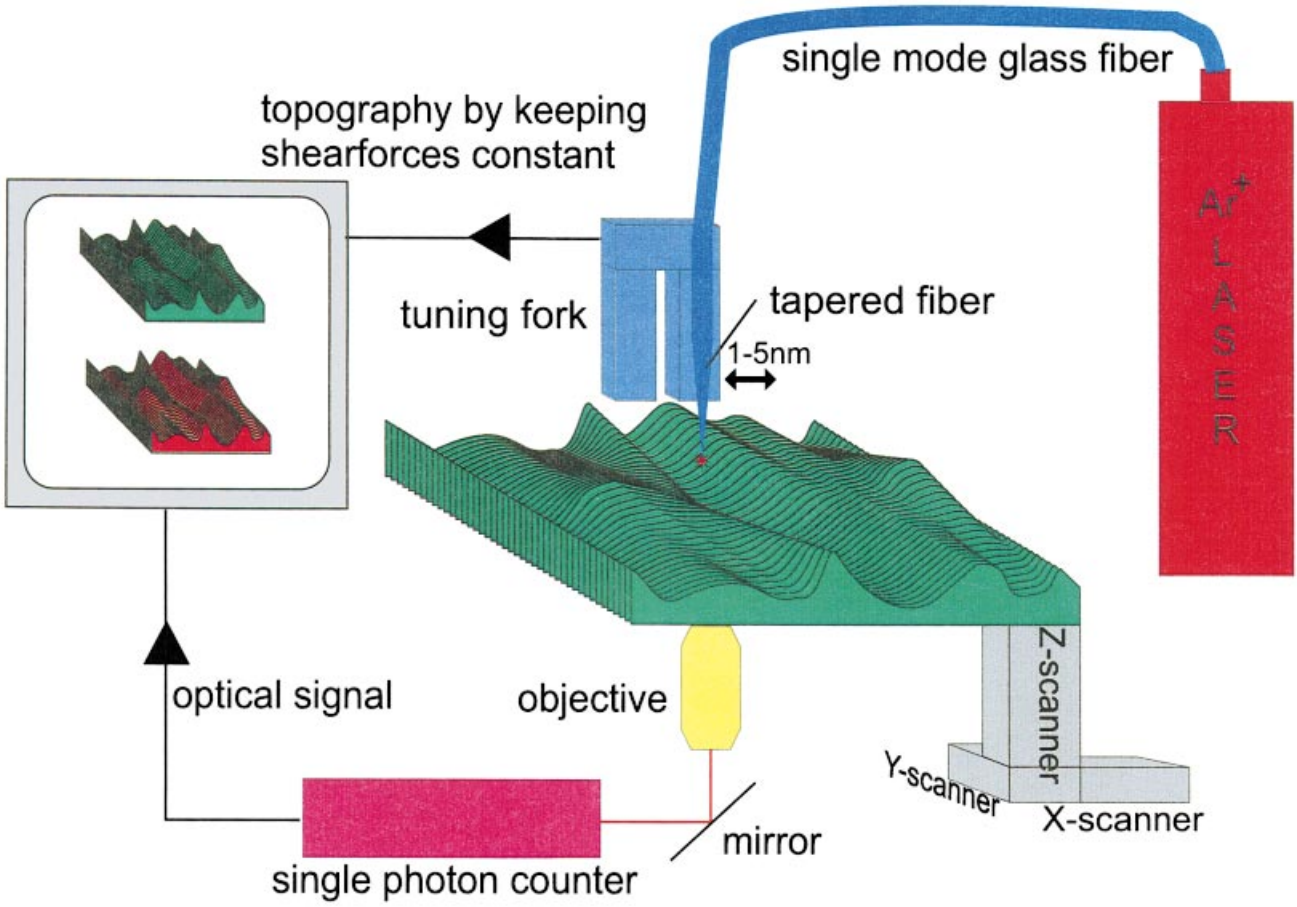


**Fig. 2.** Principle of SNOM setup in transmission mode.

resonance frequency. The probes have nominal aperture sizes at the apex of 50–100 nm in diameter. The distance control is achieved by shear-force mode (Karrai & Grober, 1995) showing the topography of the sample comparable to atomic force microscopy (AFM) (Binnig *et al.*, 1986).

An objective focused on the sample collects the emitted light. The light intensity is measured at each point of the scanning area by a single photon counting unit based on a photomultiplier tube (Hamamatsu H6240, Hamamatsu, Japan). In this way an optical image of the sample is generated.

In these experiments about 100 μW light power at 488 nm was coupled into the fibre probe to excite the fluorescent molecules. The power is attenuated at the tapered region of the fibre probe by a factor of about $10^{-3}$ supposing an aperture diameter of 100 nm (Novotny & Pohl, 1995). This leads to a power of approximately 10 nW and an intensity of $1.3 \times 10^6$ W/m$^2$ at the sample surface. A 100 × oil-objective (NA = 1.3) was used to collect the emitted light. The excitation wavelength was blocked by a long-pass filter (Schott OG515, Mainz, Germany) and a scan speed of 6 s per line and 200 × 200 pixels were chosen to collect enough fluorescent light for imaging the samples. The total acquisition time for an image is 40 min, taking into account the fact that the area is scanned in forward and reverse directions.

### *CLSM*

The investigations of the cross-sections by CLSM (Leica) were performed in reflection mode using a 63 × oil-objective (NA = 1.4), which provides the best numerical aperture. The basic principles and applications of CLSM are well described by Pawley (1993). The same area of the sample previously investigated by SNOM was found in transmission mode without fluorescence excitation by using red light (wavelength = 633 nm), in order to prevent bleaching of the fluorescent dye. After this an image was obtained by exciting the fluorescent dye with light of wavelength 488 nm. The light power at the sample surface was about 25 μW and the intensity $5 \times 10^8$ W/m$^2$ assuming a focus plane 250 nm in diameter.

## Results and discussion

The prepared samples show fluorescence in the interior of the hair fibre, as one can see in Fig. 3. The SNOM image of a

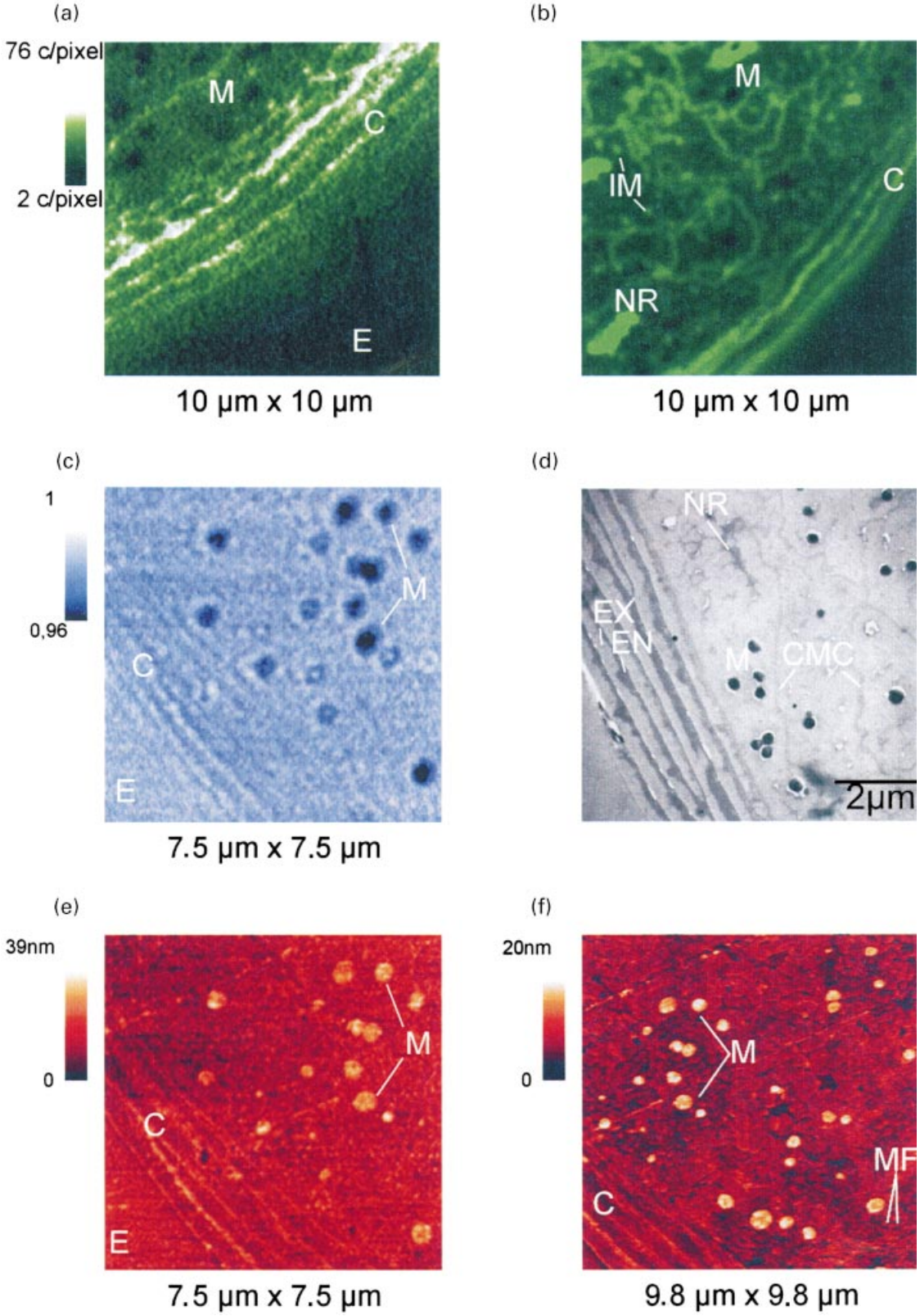
(a)
76 c/pixel
2 c/pixel
M
C
E
10 µm x 10 µm
(b)
M
IM
C
NR
10 µm x 10 µm
(c)
1
0,96
M
C
E
7.5 µm x 7.5 µm
(d)
NR
EX
EN
M
CMC
2µm
(e)
39nm
0
M
C
E
7.5 µm x 7.5 µm
(f)
20nm
0
M
MF
C
9.8 µm x 9.8 µm

50 nm thin cross-section reveals structures of the cuticule and the cortex (Fig. 3a). The image shows a weak fluorescence in the region of the hair in comparison to the Epon resin. The structural localization of the fluorescence signal suggests that the highly fluorescent regions correlate with the low sulphur parts of the hair, namely the endocuticle, the CMC, and the nuclear remnants of the cortical cells. The cuticle shows an intensely stained layered structure, because the CMC and the endocuticle act as diffusion pathways across the cuticle and take up most of the applied dye in this region of the hair. Some dark spots inside the cortex with diameters of approximately 0.5–1 μm appear in the SNOM image (Fig. 3a). Analogy with TEM images suggests that these spots are melanin pigments. The pigments of the prepared hair samples do not show any fluorescence. Either the fluorescent dye does not diffuse into the pigments or the excitation and fluorescence light is absorbed by the pigments due to the absorption capability of melanin.

Figure 3(b) represents a CLSM measurement of a 50 nm thin cross-section showing similar structures of the interior of the hair. The cross-section also shows a weak fluorescence in the hair with some brighter fluorescent parts. The network pattern of the cortex originates from the CMC that surrounds each cortical cell and acts as the diffusion pathway. The bright fluorescent regions a few micrometres in diameter within some cortical cells are associated with nuclear remnants.

Other, smaller, areas of high fluorescence inside cortical cells can also be found (indicated in Fig. 3b). These probably correspond to intermacrofibrillar material. This material is also less crosslinked and is thus able to act as the preferred diffusion pathway as reported in (Wortmann *et al.*, 1997). In addition, melanin pigments with diameters of approximately 0.5–1 μm appear in the cortex as also observed in the SNOM image (Fig. 3a).

The different morphological regions are depicted in a transmission electron microscopy (TEM) image, giving a more detailed overview of the hair structures (Fig. 3d). We have also performed a SNOM measurement in pure transmission mode at 488 nm on a 50 nm thin cross-section of an untreated hair (Fig. 3c). Some dark spots are visible, where the transmission is reduced by 3%. The spots are melanin pigments, which also appear in the SNOM topography as elevations of about 10 nm (Fig. 3e). Some elevations do not reduce the transmission signal in the transmission image. They show a dark ring with a bright centre (Fig. 3c), which may be caused by topographic influences on the optical image. Artefacts caused by topography are reported in (Hecht *et al.*, 1997).

In general, cross-sections of embedded hairs exhibit a topography which corresponds to the morphological structures of hairs. We have cross-checked this by AFM investigations of thin cross-sections, which provide a higher lateral resolution of the topography than SNOM measurements. The topography shows detailed morphological structures comparable to those observed in CLSM or TEM investigations. The fibrillar structure can be seen in the presented AFM image as well as single cuticle cells (Fig. 3f).

A CLSM image and a SNOM image of the same area of a 200 nm thin cross-section shown in Figs 4(b) and (d), respectively, indicates that the SNOM image in fluorescence mode is hardly influenced by the topography of the sample. The SNOM image reveals nearly the same structures as the CLSM image. A nuclear remnant within a cortical cell is visible in both images as a very bright fluorescent region. The molecules probably diffuse via intermacrofibrillar material towards the nuclear remnant that is located in the centre of the cortical cell as reported in (Wortmann *et al.*, 1997). The nuclear remnant of the hair is also a very low sulphur region. We suppose either that the nuclear remnants swell during penetration more than the other parts of the cortex, and thus take up more molecules, or the nuclear remnants have a higher binding-affinity for the dye.

However, the nuclear remnants appear much brighter in the images. In this case the topography provides additional information about the sample, which can be very helpful for interpretation of the fluorescence image. The bright fluorescence of the nuclear remnants cannot be explained by an increased sample thickness of this region, because this part is actually much thinner than the rest of the sample.This suggests an increased dye uptake of the nuclear remnants (Figs 4c and d).

The SNOM images show an identical network pattern to that in the CLSM image. Each cortical cell is surrounded by the CMC and thus the network pattern corresponds to the cell borders. The variety of cell size and shape which occurs in the images is due to natural variation and surely depends

**Fig. 3.** Comparison of different imaging modes. (a) SNOM fluorescence image of a 50 nm thin cross-section of a hair embedded in Epon after penetration of a fluorescent dye. The structures are similar to those seen in the CLSM image (b). (b) CLSM image of a 50 nm thin cross-section of the same hair embedded in Epon showing diffusion pathways of the dye into the interior of the hair. (c) SNOM transmission image of a 50 nm cross-section of an untreated human hair embedded in Epon. (Wavelength = 488 nm). (d) TEM image of a 50 nm thin cross-section of a hair after embedding in Epon and staining with uranyl acetate. (e) SNOM topography belonging to (c). (f) AFM topography of the sample, shown in (c) and (e). The topography correlates with the morphology of hairs, which is better resolved in AFM than in SNOM. M = melanin pigment, C = cuticle, NR = nuclear remnant, IM = intermacrofibrillar material, MF = macrofibril, E = Epon, EX = exocuticle, EN = endocuticle, CMC = cell membrane complex.

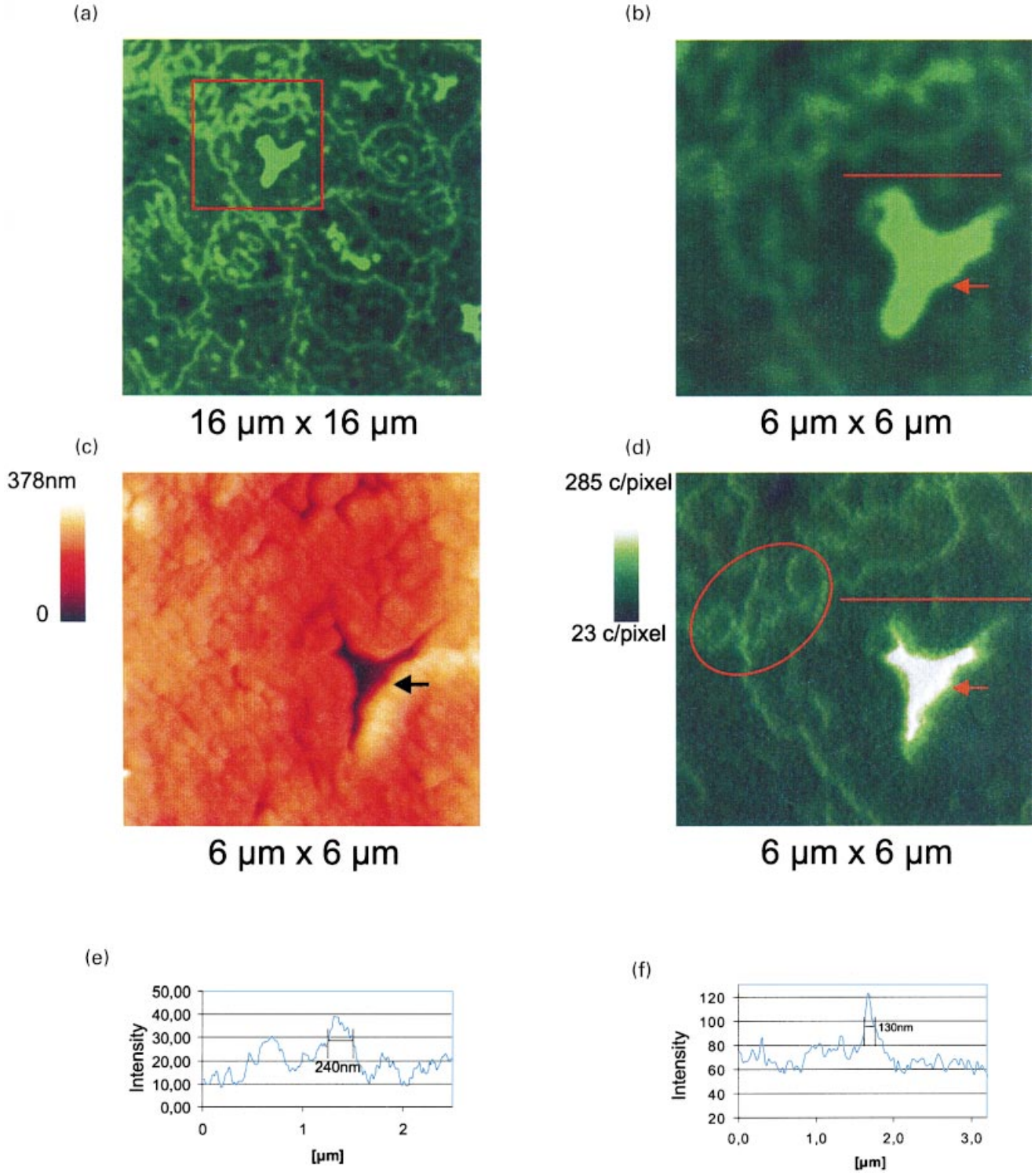


**Fig. 4.** A 200 nm thin cross-section of a hair embedded in Epon after penetration of a fluorescent dye. The CLSM image (a) shows a network of diffusion pathways of the dye in the cortex of the hair. Zoom (b) of CLSM image of the area that was previously measured by SNOM. The cross-section is thinner at the nuclear remnant (←) in the SNOM topography (c) and appears bright in the SNOM fluorescence image (d). Small structures originate from the fringes of each cortical cell (marked area in d). (e) and (f) present line profiles of the areas indicated in (b) and (d), respectively.

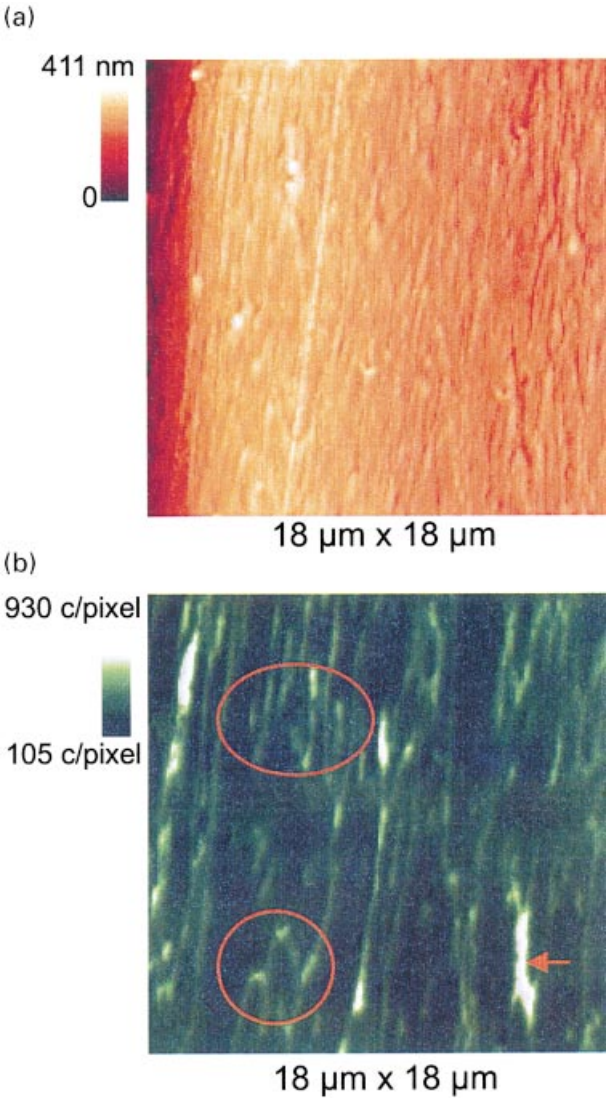


**Fig. 5.** SNOM topography (a) and fluorescence image (b) of a longitudinal section (200 nm) of a hair embedded in Epon after penetration of a fluorescent dye. Cortical cell structures occur, especially fringes (marked areas) and nuclear remnants (←).

on the position of the plane of cutting. The small structures are probably cell protrusions or interdigitations between two cortical cells (marked areas in Figs 4d and 5b).

The SNOM image clearly provides a higher lateral resolution than the CLSM image. Therefore, in some regions of the sample the pathways can be better separated from each other in the SNOM image than in the CLSM image. The full width half maximum (FWHM) of a small structure within the cortex cell is approximately 240 nm in the CLSM image (Fig. 4e), nearly the theoretical resolution of 225 nm according to the Rayleigh criterion (with $\lambda = 518$ nm and NA = 1,4). The resolution obtained in the SNOM image is approximately 130 nm, estimated by determing the FWHM of the signal of the identical structure (Fig. 4f). This resolution is clearly higher than the theoretical resolution limit in conventional light microscopy and the resolution of the CLSM measurement.

It should be noted that bleaching effects induced by the previous SNOM measurement do not occur in the CLSM image (Fig. 4a). The area which was previously investigated by SNOM exhibits the same fluorescence intensity as the surrounding region in the CLSM image. Therefore, we believe that the light intensity in the SNOM measurement was low enough to prevent bleaching. We checked this by measuring an area of another sample twice with the same measurement parameters (not presented here). Although the investigated area was scanned in forward and reverse directions in the first measurement, no significant reduction in the fluorescence signal was observed in the second measurement. This is an important prerequisite for comparative measurements of the same area by SNOM and CLSM with respect to resolution capabilities.

We also investigated thin longitudinal sections of hair treated using the same procedure. Figures 5(a) and (b) represent a SNOM measurement of a 200 nm thin longitudinal section. In Fig. 5(b) fluorescence labelled elongated structures of cortical cells can be found. At the bottom right of the image a bright fluorescent region can be observed; this is a nuclear remnant. In the indicated areas a structure can be observed that is probably associated with the fringes of cortical cells. In this region two cortical cells obviously interdigitate. This image explains the observed structures of the cross-sections presented above. The size and shape of the cell borders, which appear in a cross-section, strongly depend on the position of the cutting plane. A schematic drawing of a longitudinal plane of a hair shows the different cell structures which are possible (Fig. 1c).

## Conclusion

The penetration of octadecanoylaminofluorescein into human hairs follows the rules of diffusion theory described above. The dye molecules penetrate the cuticle via the endocuticle and CMC, reaching the cortex. The CMC of the cortical cells also functions as the preferred diffusion pathway, explaining the observed network pattern of the cortex. The weak fluorescence inside each cortical cell can be explained by the extreme penetration conditions chosen in these experiments. Longer penetration times and higher temperatures lead to a migration of molecules into cortical cells and nuclear remnants (Kamath *et al.*, 1995).

The topography does not seem to play an important role in the contrast mechanism of the SNOM measurements in fluorescence mode, unlike in pure transmission mode reported by Hecht *et al.* (1997).

Although we do not use a pinhole in front of the detector we can achieve a resolution below the diffraction limit. A pinhole is often used in other SNOM setups to reduce

out-of-focus light (Hecht *et al.*, 1997), and this decreases the resolution capability. For the investigation of thin sections it is obviously not necessary to use a pinhole, as our results demonstrate.

## Outlook

SNOM offers a possible way to describe diffusion pathways of fluorescent dyes into hair fibres at a resolution below the diffraction limit (~100 nm), as we have demonstrated above. In particular, the diffusion across the cuticle is of high interest, because of its importance with regard to cosmetic treatments. It should be possible in the future to study the penetration of ingredients of hair care products linked with a fluorescent marker molecule.

## Acknowledgements

We thank Dr F. Pflücker for the TEM measurement. Financial support from the BMBF (grant no. 13N6921/3) is gratefully acknowledged.

## References

Betzig, E. & Trautmann, J.K. (1992) Near-field optics. Microscopy, spectroscopy, and surface modification beyond the diffraction limit. *Science*, **257**, 189–195.

Binnig, G., Quate, C.F. & Gerber, Ch. (1986) Atomic force microscopy. *Phys. Rev. Lett.* **56**(9), 930–932.

Corcuff, P., Grememillet, P., Jourlin, M., Duvault, Y., Leroy, F. & Leveque, J.L. (1993) 3D reconstruction of human hair by confocal microscopy. *J. Soc. Cosmet. Chem.* **44**, 1–12.

Dürig, U., Pohl, D.W. & Rohner, F. (1986) Near-field optical-scanning microscopy. *J. Appl. Phys.* **59**(10), 3318–3327.

Hecht, B., Bielefeldt, H., Inouye, Y., Pohl, D.W. & Novotny, L. (1997) Facts and artifacts in near-field microscopy. *J. Appl. Phys.* **81**(6), 2462–2498.

Kamath, Y., Bradford, I., Hornby, S., Ramaprasad, K., Ruetsch, S. & Weigmann, H.D. (1995) Analysis and quantification of hair damage. *Prog. Report TRI Princeton*, **9**, 20–31.

Kaplin, I.J., Schwan, A. & Zahn, H. (1982) Effects of cosmetic treatments on the ultrastructure of hair. *Cosmet. Toilet.* **97**, 22–26.

Karrai, K. & Grober, R.D. (1995) Piezoelectric tip-sample distance control for near field. *Appl. Phys. Lett.* **66**(14), 1842–1844.

Kassenbeck, P. (1991) *The Hair and its Structure.* Wella AG, Darmstadt, Germany.

Novotny, L. & Pohl, D.W. (1995) Light propagation in scanning near-field optical microscopy. *Photons and Local Probes* (ed. by O. Marti and R. Möller), p. 21. Kluwer, Dordrecht.

Pawley, J.B. (1993) *Handbook of Biological Confocal Microscopy.* Plenum Press, New York.

Pohl, D.W., Denk, W. & Lanz, M. (1984) Optical stethoscopy: image recording with resolution λ/20. *Appl. Phys. Lett.* **44**(7), 651–653.

Pötsch, L. & Moeller, M.R. (1996) On pathways for small molecules into and out of human hair fibers. *J. Forensic Sci.* **41**(1), 121–125.

Robbins, C.R. (1988) *Chemical and Physical Behavior of Human Hair.* Springer Verlag, New York, p. 151.

Shotton, D.M. (1989) Confocal scanning optical microscopy and its applications for biological specimens. *J. Cell Sci.* **94**, 175–206.

Wortmann, F.J., Wortmann, G. & Zahn, H. (1997) Pathways for dye diffusion in wool fibers. *Textile Res. J.* **64**(10), 720–724.

Zahn, H. (1984) Feinbau und Chemie des Haares. *Parfümerie Kosmetik*, **63**, 507–523, 585–590.

Zahn, H., Wortmann, F.J. & Höcker, H. (1997) Chemie und Aufbau der Wolle. *Chemie Unserer Zeit*, **31**(6), 280–290.